Journal of Luminescence 197 (2018) 349–353

Contents lists available at ScienceDirect

Journal of Luminescence

journal homepage: www.elsevier.com/locate/jlumin

Mid-infrared spectroscopy of Pr-doped materials

Brian M. Walsh[a,*], Uwe Hommerich[b], Akira Yoshikawa[c], Alessandra Toncelli[d]

[a] NASA Langley Research Center, Hampton, VA 23681, USA
[b] Department of Physics, Hampton University, Hampton, VA 23668, USA
[c] Institute for Materials Research, Tohoku University, Sendai 980-8577, Japan
[d] NEST, CNR Istituto Nanoscienze and Dipartimento di Fisica, Università di Pisa, Pisa 56127, Italy

ARTICLE INFO

Keywords:
Praseodymium
Low phonon materials
Fluorides
Chlorides
Bromides
Mid-infrared
spectroscopy
Lasers

ABSTRACT

Solid state lanthanide doped lasers primarily operate in the ultraviolet, visible, near infrared and short-wavelength infrared out to around 2.1 μm. At longer wavelengths, the transitions in conventional oxide crystal and glass materials become susceptible to multiphonon quenching due to their relatively large phonon energy. The use of low phonon materials can minimize the nonradiative quenching, opening up possibilities for solid state lanthanide lasers operating in the mid-infrared (MIR). This provides motivation to study the spectroscopy of lanthanide ions in bromide, chloride and fluoride materials, which have relatively low phonon energies. In this article, the MIR spectroscopy or praseodymium ions in five different host materials is studied, specifically KPb_2Br_5 (KPB), LaF_3, KYF_4 (KYF), BaY_2F_8 (BYF) and $YLiF_4$ (YLF) host crystals. The MIR emission cross sections have been measured from 3 to 6 μm and reciprocity of absorption and emission is utilized to validate the results. The lifetime dynamics in the MIR are covered for various pump and emission wavelengths. Results are also presented on MIR emission from 6.5 to 8.5 μm in a Pr: KPB crystal, which, to the best of the authors knowledge, is the first such measurement of luminescence in this wavelength range that has been published.

1. Introduction

Most lanthanide doped solid-state materials can produce laser wavelengths in the near-infrared (NIR) from 0.75 to 1.4 μm, or short wavelength infrared (SWIR) from 1.4 to 3 μm. However, it becomes increasingly difficult to generate wavelengths in the mid-wavelength infrared (MWIR) from 3 to 8 μm and beyond. We use the term mid-infrared (MIR) to specifically refer to the MWIR wavelength range [1]. The great challenge in solid-state lasers for MIR operation is finding materials that offer low phonon energies. Solid-state lasers that have wavelengths longer than about 3 μm are usually quenched by nonradiative processes, resulting from the generation of phonons, which are the quanta of the crystal lattice vibrations. When the energy gap between two adjacent manifolds is less than about 5 times the maximum phonon energy, the nonradiative transitions results in luminescence quenching of the upper manifold. Hence, developing efficient MIR lasers with wavelengths longer than about 3 μm requires host materials with relatively low phonon energy. These typically include halide crystals (bromide, chloride and fluoride), sulfides (thiogallates) and glass materials like chalcogenides that can also be used.

Towards developing viable lasers in the MIR, we have investigated the spectroscopy of Praseodymium (Pr^{3+}) ions in five host materials from 3 to 6 μm. The host materials investigated are KPb_2Br_5 (KPB), LaF_3, KYF_4 (KYF), BaY_2F_8 (BYF) and $YLiF_4$ (YLF), which have maximum phonon energies of 138, 392, 350, 415 and 490 cm^{-1}, respectively [2–6]. The Pr emission from 3 to 6 μm is complicated by the fact that several different possible channels for the emission exists, including the $^3F_4 \rightarrow {}^3F_2$, $^3F_3 \rightarrow {}^3H_6$, $^3H_6 \rightarrow {}^3H_5$ and $^3H_5 \rightarrow {}^3H_4$. To narrow the contributing channels, pump sources at 1.55 μm and 1.9 μm were used to excite the samples, but there was virtually no difference in the observed spectra. The 3–6 μm Pr emission, therefore, is likely due to just the $^3H_6 \rightarrow {}^3H_5$ and the $^3H_5 \rightarrow {}^3H_4$ transitions. The measurements conducted include emission cross sections and lifetime dynamics. Reciprocity of absorption and emission is also used to validate the emission measurements with good agreement being found for all materials investigated.

Regarding applications, laser demonstrations in the MIR remain in their infancy, with very few examples to date. Efforts to develop MIR lanthanide based solid state lasers can be of substantial benefit in producing sources for the spectral ranges 3–8 μm, a region that is rich in many atmospheric molecular gasses [1]. The impact is clear, and in the MIR region, broad spectral coverage buys access to chemical

* Corresponding author.
E-mail address: brian.m.walsh@nasa.gov (B.M. Walsh).

https://doi.org/10.1016/j.jlumin.2018.01.032
Received 1 December 2017; Accepted 18 January 2018
Available online 02 February 2018
0022-2313/ Published by Elsevier B.V.

Table 1
Atomic and crystallographic parameters.

Crystal Formula	Crystal Name	Crystal System	Space Group	Dopant Site	N_c	N_f	Lattice Parameters (Å)			Angular Parameters			N_S (x10^{22} cm^{-3})
							a	b	c	α	β	γ	
KPb_2Br_5	KPB	Monoclinic	14	Pb^{2+}	2	4	9.256	8.365	13.025	90	~ 90	90	0.793
LaF_3	LaF3	Trigonal	165	La^{3+}	1	6	7.185	–	7.351	90	90	120	1.826
KYF_4	KYF	Trigonal	144	Y^{3+}	1	18	14.060	–	10.103	90	90	120	1.041
BaY_2F_8	BYF	Monoclinic	12	Y^{3+}	2	2	6.983	10.519	4.264	90	99.7	90	1.304
$YLiF_4$	YLF	Tetragonal	88	Y^{3+}	1	4	5.166	–	10.733	90	90	90	1.396

"fingerprints," where molecules can be detected and distinguished with great sensitivity. In fact, the region of the MIR from 3 to 5 μm is one of the "fingerprint regions" of interest for remote sensing.

2. Low phonon materials

The Pr-doped crystalline materials studied in this article were chosen for their relatively low phonon energies [2–6]. They consist of 1 bromide (KPB) and 4 fluorides (LaF_3, KYF, BYF and YLF). In the case of the fluoride crystals, the Pr^{3+} ions substitute for La^{3+} in LaF_3, and Y^{3+} in KYF, BYF and YLF. For the bromide crystals (KPB), the Pr^{3+} ions substitute for Pb^{2+} with charge compensation. There are two nonequivalent octahedral sites for the Pb^{2+} ions, but the predominant one is observed to be octahedral with a coordination number of CN = 6. The KPB and BYF crystals are biaxial, while the LaF_3, KYF and YLF crystals are uniaxial. Table 1 gives the crystallographic and atomic parameters for KPB, LaF3, KYF, BYF and YLF [7–11]. In this table, N_c is the number of atoms in the atomic formula of the crystal for which the dopant ion replaces, N_f is the number of formula units per unit cell of the crystal. The lattice parameters of the unit cell are a, b, c, and the angular parameters of the unit cell are α, β, γ. These parameters can be used to calculate the site density, N_S, of the available dopant sites as follows:

$$N_S = \frac{N_c N_f}{V_c} \tag{1}$$

where V_c is the volume of the unit cell. For monoclinic crystals, V_c = abc(sin β), for trigonal crystal symmetry with hexagonal axes, $V_c = (3/4)^{1/2}a^2c$, and for tetragonal crystals, $V_c = a^2c$. From these formulas for V_c and the values of N_c and N_f, the site densities, N_S, are calculated in Table 1. The concentration density of the dopant ions, N_D, is then found by multiplying the fractional concentration, C_S, by the site density, that is, $N_D = C_S N_S$, in units of 1/cm^3.

3. Experiment

Transmission spectra were recorded with a Perkin-Elmer Frontier Optica FT-IR spectrophotometer in the range 3–6 μm at room temperature. A wire grid polarizer was used in the sample chamber to record polarized spectra. The transmission data was corrected for Fresnel losses at the sample faces and used to obtain the absorption cross section. For continuous luminescence measurements, a 1.5 μm erbium doped fiber amplifier (EDFA) and a 1.9 μm diode laser were used as pump sources. The collected luminescence was focused by a CaF_2 lens on the slit of a 0.5-meter SPEX monochromator after passage through a chopper providing the reference signal for a lock-in amplifier. The grating was 150 gr/mm blazed at 5.0 μm. Detection of the signal was achieved with a liquid nitrogen cooled Judson J15D12 mercury cadmium telluride (MCT) detector. A Stanford Research Systems model SR530 DSP lock-in amplifier was used for signal amplification and digitization. The digitized signal was collected by scanning software on the computer for storage. Polarization selection of the luminescence signal was achieved by placing a wire grid polarizer between the focusing lens and the entrance slit of the spectrometer. Appropriate cut-off filters discriminated against wavelengths below ~3 μm. A Mercury (Hg) lamp was used to calibrate the wavelength and an Oriel blackbody source, model 67036, was used to correct for grating efficiency, detector response and other optical elements of the system. Lifetimes were measured using a VIBRANT (HE) 355 II OPO pulsed laser source, tunable from 0.4 to 2.4 μm, and an MCT detector and amplifier combination signal was processed by a digital oscilloscope for storage. Narrow band filters were used to select the wavelength of the luminescence. Concentrations of the Pr doping is 1.0%, 1.5%, 1.25%, 1.0% and 1.0% in KPB, LaF3, KYF, BYF and YLF samples, respectively.

4. Results

The most general form for the emission cross section using the beta-tau method is the following [12],

$$\sigma_p(\lambda) = \frac{\lambda^5}{8\pi c n^2 (\tau_r/\beta)} \frac{I_p(\lambda)}{\int \frac{1}{3}[I_a(\lambda) + I_b(\lambda) + I_c(\lambda)]\lambda d\lambda} \tag{2}$$

where p is the polarization. n is the index of refraction, τ_r is the radiative lifetime and β is the branching ratio, For isotropic crystals a = b = c, while for uniaxial crystals a = b, and for biaxial crystals a, b and c are unique. The crystals in this study are uniaxial and biaxial. For the case of uniaxial crystals there is π (E || c) and σ (E ⊥ c) polarization, denoting whether the electric field of the luminescence is parallel to or perpendicular to the c-axis, respectively. For biaxial crystals, there are E || a, E || b and E || c, denoting the polarizations for the electric field of the luminescence parallel to the respective axis.

The absorption cross sections for a given polarization is determined with knowledge of the dopant concentration and absorption path length according to [12],

$$\sigma_{abs}(\lambda) = -\frac{1}{C_S N_S l} ln\left[\left(\frac{n^2+1}{2n}\right)T(\lambda)\right] \tag{3}$$

where N_S is the site density available to the dopant ion, C_S is the fractional dopant concentration in percent/100, l is the absorption path length, n is the index of refraction, and $T(\lambda)$ is the transmission of the sample as measured by the spectrophotometer. The factor $(n^2+1)/2n$ accounts for the Fresnel reflections at the surfaces of the crystal. Refractive index values are found in the literature [2,12–14]. Values for KYF were not available, so refractive index values for YLF were used instead.

The emission and absorption cross sections are related through a reciprocity relation requiring some knowledge of the energy levels of the ground state manifold and an excited state manifold [12],

$$\sigma_{em}(\lambda) = \sigma_{abs}(\lambda)\frac{Z_l}{Z_u}\exp\left(\frac{E_{ZL} - hc/\lambda}{kT}\right) \tag{4}$$

where Z_l and Z_u are the partition functions of the lower and upper manifolds, respectively. E_{ZL} is the zero-line energy, defined as the energy difference between the lowest Stark levels of the upper and lower manifolds. k is Boltzmann's constant and T is the temperature.

Polarized emission spectra were measured in the region from 3 to 6 μm. The spectra were corrected for system response (grating efficiency, detector response and other elements of the collection system)

Table 2
Pr-doped material parameters.

Material	Z_l / Z_u	E_{ZL} (cm^{-1})	Judd-Ofelt Parameters ($x10^{-20}$ cm^2)			τ_r (ms)
			Ω_2	Ω_4	Ω_6	
KPb_2Br_5	0.925	2178	8.63	6.11	1.94	40
LaF_3	0.925	2178	0.13	0.70	9.60	72
KYF_4	0.742	2253	3.92	1.78	7.94	106
BaY_2F_8	0.676	2175	0.00	10.47	12.90	56
$YLiF_4$	0.742	2253	0.00	8.07	7.32	104

with a blackbody source, and the emission cross section calculated using Eq. (2). Since the KPB sample was unoriented with respect to the a, b, and c axes, only the unpolarized emission was measured. The radiative lifetimes for Pr-doped KPB, KYF, BYF and YLF were obtained from Judd-Ofelt (JO) parameters available in the literature [15–18], while for Pr:LaF3 an independent JO analysis was done. Polarized transmission spectra were measured from 3 to 6 μm, corrected for Fresnel reflections at the surface ends and absorption cross sections calculated using Eq. (3) with knowledge of the site density, N_S, fractional Pr concentration, C_S, and path length of the sample, l. Just as with emission, the KPB sample transmission spectra was unpolarized for the same reason as in the emission studies. The absorption spectra were used to produce derived emission spectra from the reciprocity relation in Eq. (4), using relevant parameters given in Table 2. The parameters used require information on the energy levels for Pr-doped KPB, LaF_3, KYF, BYF and YLF [19–21]. Values for energy levels of Pr:LaF_3 and Pr:YLF were used for Pr:KPB and Pr:KYF, respectively, due to lack of data for the later.

Overall, there is good agreement between the measured emission cross sections and those derived from absorption. Fig. 1 shows the absorption cross section, emission cross section and emission derived from absorption for Pr:LaF_3 with π-polarization. The absorption spectra are due to the transition from the ground state to the first excited state, i.e., the $^3H_4 \rightarrow {}^3H_5$ transition. As noted in the introduction, however, several possible channels for the emission exist, depicted in the energy level diagram in Fig. 2. Pump sources at 1.55 μm and 1.91 μm were used to excite the Pr-doped samples, but there was virtually no difference in the observed emission spectra. The Pr emission in the crystals studied, therefore, is likely solely due to just the $^3H_6 \rightarrow {}^3H_5$ and the $^3H_5 \rightarrow {}^3H_4$ transitions, and predominantly the later.

The measured emission cross section and those derived from absorption were also compared for Pr:KPB, Pr:KYF, Pr:BYF and Pr:YLF. The spectra are shown in Figs. 3–6, but without the absorption cross section for clarity of presentation. Just as for LaF_3, the agreement is quite good in overall shape of the spectra. The spectra of Pr:YLF for the derived emission is unusual on the long wavelength side in rising off

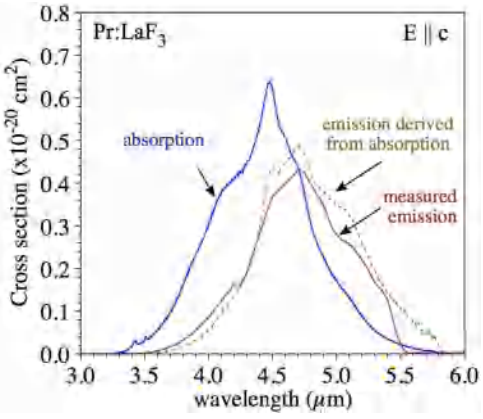

Fig. 1. Cross sections for Pr:LaF_3, π-polarization.

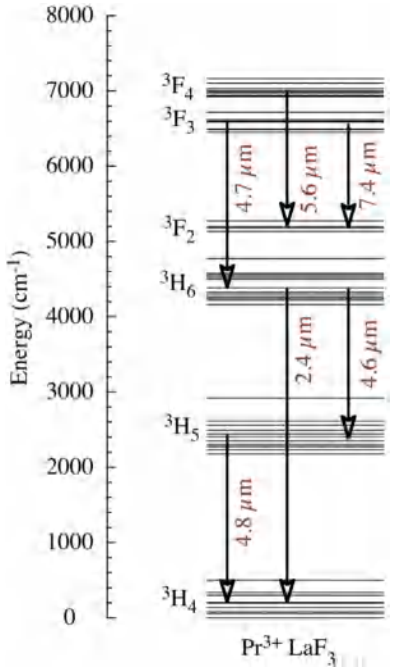

Fig. 2. Energy level diagram for Pr:LaF_3.

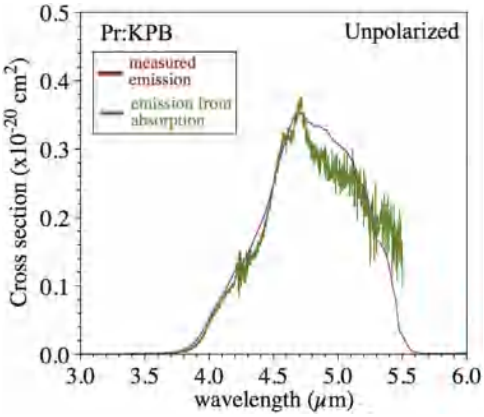

Fig. 3. Emission cross section of Pr:KPB, unpolarized.

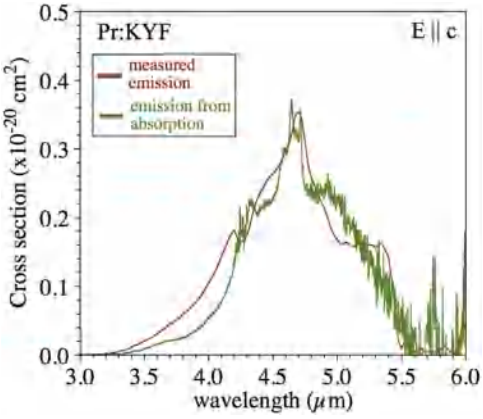

Fig. 4. Emission cross section of Pr:KYF, π-polarization.

scale. This appears to be due to reaching the lattice absorption edge in this particular crystal.

The lifetime dynamics were examined under pumping at 1.55 μm and 1.91 μm, corresponding to the $^3F_3$ and $^3F_2$ manifolds, respectively.

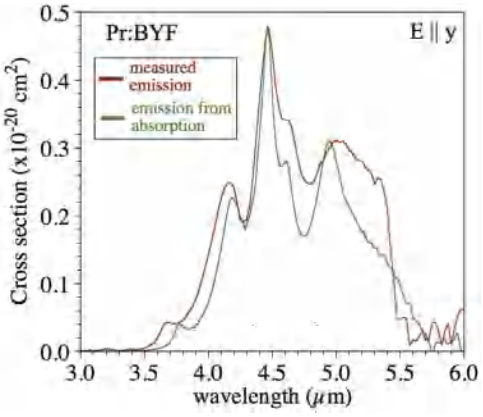

Fig. 5. Emission cross section of Pr:BYF, E || y.

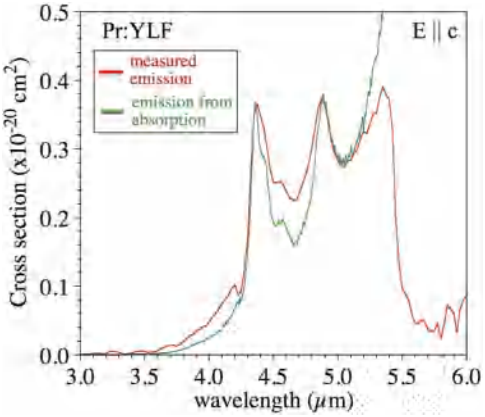

Fig. 6. Emission cross section of Pr:YLF, π-polarization.

Narrow band (NB) and long pass (LP) filters were used to discriminate in favor of a particular emission wavelength. Due to the weak signal available for these measurements, focus is given to the Pr:KPB sample, which has the lowest phonon energy of the Pr-doped samples studied. For pump wavelength (λ_P) at 1.55 μm, emission (λ_E) was seen at 1.6 μm, 2.4 μm, 4.7 μm and 7.4 μm. Pumping at 1.91 μm, emission was seen at 2.4 μm and 4.7 μm. The results of these lifetime measurements are summarized in Table 3.

The results for the lifetime measurements are consistent with what would be expected. The $^3F_3$ lifetimes with 1.55 μm pumping for both the 1.6 μm and 7.4 μm transitions are approximately the same, as they should be. The $^3H_6$ and $^3H_5$ lifetimes for pumping at 1.55 μm and 1.9 μm are the same, as is also to be expected. These measured lifetimes (τ) can be compared with radiative lifetimes (τ_r) from the Judd-Ofelt theory using the Judd-Ofelt parameters for Pr: KPB in Table 2. The Judd-Ofelt values of the radiative lifetimes for the $^3F_3$, $^3H_6$ and $^3H_5$ manifolds are 0.5 ms, 20 ms, and 40 ms, respectively. These agree reasonably well with the measured lifetimes of 0.4 ms, 15 ms and 37 ms for the $^3F_3$, $^3H_6$ and $^3H_5$ manifolds as shown in Table 3. The measured lifetime curves are shown in Fig. 7 on a log scale.

Table 3
Emission lifetime measurements for Pr: KPB.

λ_P (μm)	Pump transition	λ_E (μm)	Emission transition	τ (ms)	Filter
1.55	$^3H_4 \rightarrow {}^3F_3$	1.6	$^3F_3 \rightarrow {}^3H_4$	0.42	NB1600
		2.4	$^3H_6 \rightarrow {}^3H_4$	15.0	NB2470
		4.7	$^3H_5 \rightarrow {}^3H_4$	37.0	LP4000
		7.4	$^3F_3 \rightarrow {}^3F_2$	0.40	LP6210
1.91	$^3H_4 \rightarrow {}^3F_2$	2.4	$^3H_6 \rightarrow {}^3H_4$	15.0	NB2470
		4.7	$^3H_5 \rightarrow {}^3H_4$	37.0	LP4000

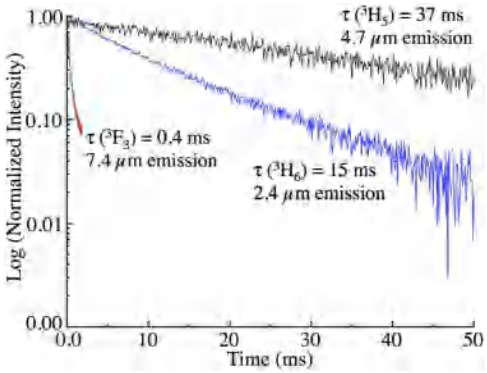

Fig. 7. Emission decay log plot curves for Pr:KPB.

An interesting aspect of the lifetime measurement was the detection of emission from the $^3F_3$ manifold at 7.4 μm. It was only observed when pumping at 1.55 μm directly into the $^3F_3$ manifold, but not when pumping at 1.91 μm into the $^3F_2$ manifold. This provided some incentive to endeavor a measurement of the emission spectrum also. This required a special grating, 120 gr/mm blazed at 7.7 μm, which facilitated detection. To the best of the authors knowledge, this is the first such observation of an emission spectrum in Pr-doped materials for the $^3F_2 \rightarrow {}^3F_3$ transition in the 7 μm region for halide crystals, shown in Fig. 8.

Bowman, et al. [22], has demonstrated laser action at 7 μm in Pr: $LaCl_3$ originating from the $^3F_3$ manifold, but no emission spectrum in this wavelength region was reported in the article. The lifetime of the emission was measured, however, and reported to be 0.9 ms. It is interesting that Bowman, et al., observed upconversion to the $^3F_3$ manifold while pumping with 1.9 μm. We did not observe this in our lifetime measurements pumping at 1.91 μm in Pr: KPB, though our OPO pump source only generated < 10 mJ, perhaps insufficient to see the upconverted emission signal.

The emission spectrum reported here in the 7 μm wavelength region for Pr:KPB has approximately the correct wavelength span that would be expected. Since the energy levels for Pr:KPB are not available, Pr:LaF3 energy levels can be used to estimate the approximate expected span in wavelength. For LaF_3, the Stark levels range from 6450 to 6719 cm^{-1} for the $^3F_3$ manifold and 5134 to 5276 cm^{-1} for the $^3F_2$ manifold. From these energy level values, the range of expected wavelengths for the $^3F_3 \rightarrow {}^3F_2$ transition is calculated to be 6.3 to 8.5 μm, which agrees fairly well with the observed emission spectra of Pr:KPB in Fig. 8. Unlike the $^3H_5 \rightarrow {}^3H_4$ spectrum for Pr:KPB in Fig. 3, reciprocity can not be used as a check on the shape of the spectrum since the 7 μm transition does not terminate on the ground state. Nevertheless, the lifetime measurements and the wavelength span give a level of

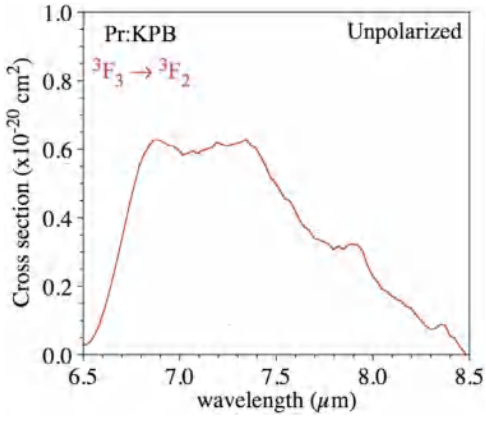

Fig. 8. $^3F_3 \rightarrow {}^3F_2$ emission spectrum in Pr:KPB.

confidence to the results.

5. Summary

The MIR spectroscopy for five Pr-doped crystals has been investigated. The crystal hosts are KPb_2Br_5 (KPB), LaF_3, KYF_4 (KYF), BaY_2F_8 (BYF) and $YLiF_4$ (YLF). Emission and absorption cross sections were measured in the 3–6 μm wavelength region. Derived emission spectra were produced from the reciprocity of absorption. This provided a way to validate the measured MIR emission spectra, since the spectral landscape here remains relatively unexplored and there are few examples to rely on as a basis of comparison. Transient decay measurements were also performed to asses the excitation dynamics and lifetime of the $^3H_5$, $^3H_6$, and $^3F_3$ manifolds. The results for the lifetimes are self-consistent for the Pr:KPB sample, and in fair agreement with radiative lifetimes determined from Judd-Ofelt parameters utilized.

In addition to the measurements in the 3 – 6 μm MIR wavelength region, the emission from 6.5 to 8.5 μm region in Pr:KPB has been measured, and supporting evidence for its validity is given. The evidence mainly relies on lifetime measurements and the span of the spectral range, which indicate this is emission from the $^3F_3 \rightarrow {}^3F_2$ transition. To the best of the author's knowledge, this is the first such measurement of ~ 7 μm emission spectra in lead halide crystals, though laser action was demonstrated near 7 μm in a Pr:$LaCl_3$ crystal over 20 years ago [22].

In a sense, this study overall is a first of its kind in the MIR spectral region from 3 to 8 μm, in that it does not focus on a particular crystal structure, but examines Pr^{3+} ions in five different low phonon crystal structures. This is important to assess the potential of various low phonon hosts for laser action in the MIR. It provides inspiration for the exciting prospect of developing lasers at such long wavelengths and utilizing them in various applications, such as remotes sensing or defense and security.

When the laser was first invented in the 1960's, it was said to be an invention in search of an application. Today, the reverse is true and applications are in search of lasers. Though a small sector of the laser market, MIR lasers have been one of the fastest growing in recent years. There is a wide spectral landscape from 3 to 8 μm open to exploration and MIR solid state lasers can certainly play a role in offering laser devices where there is a need for various applications. The challenge ahead is to advance MIR laser devices to offer viable advantages and alternatives to conventional IR lasers traditionally operating the 1–2 μm wavelength region.

From a research and development perspective, the field of spectroscopy and lasers in the MIR is a relatively new field of study evolving over the last 20 years and driven by advances in development of low phonon hosts such as lead halide crystals (i.e., KPb_2Br_5, $RbPb_2Cl_5$), thiogallate crystals (i.e., $CaGa_2S_4$, $PbGa_2S_4$), and chalcogenide glasses (i.e., $Ge_{30}As_{20}Se_{50}$). This has provided the motivation to study new materials that meet new objectives.

References

[1] B.M. Walsh, H.R. Lee, N.P. Barnes, J. Lumin. 169 (2016) 400.
[2] K. Rademaker, W.F. Krupke, R.H. Page, S.A. Payne, K. Petermann, G. Huber, A.P. Yelisseyev, L.I. Isaenko, U.N. Roy, A. Burger, K.C. Mandal, K. Nitsch, J. Opt. Soc. Am. B 21 (2001) 2117.
[3] H.H. Caspers, R.A. Buchanan, H.R. Martin, J. Chem. Phys. 41 (1964) 94.
[4] S. Veronesi, B. Parisi, R. Faoro, M. Toncelli, J. Lumin. 132 (2012) 2307.
[5] A.A. Kaminskii, S.E. Sarkisov, F. Below, H.J. Eichler, Opt. Quant. Electron. 22 (1990) S95.
[6] H.H. Caspers, H.E. Rast, J. Lumin. 10 (1975) 347.
[7] A.A. Merkulov, L.I. Isaenko, V.M. Pashkov, V.G. Mazur, A.V. Virovets, D.Yu Naumov, J. Struct. Chem. 46 (2005) 103.
[8] A. Zalkin, D.H. Templeton, T.E. Hopkins, Inorg. Chem. 5 (1966) 1466.
[9] Y. Le Fur, N.M. Khaidukov, S. Aleonard, Acta Cryst. C48 (1992) 978.
[10] L.H. Guilbert, J.Y. Gesland, A. Bulou, R. Retoux, Mater. Res. Bull. 28 (1993) 923.
[11] C.A. Morrison, R. Levitt, in Handbook on the Physics and Chemistry of Rare Earths, eds. K.A. Gschneidner, Jr., and L. Eyring, North Holland, NY, Volume 5, Chap. 46, 1982, p. 626.
[12] B.M. Walsh, N.P. Barnes, B. Di Bartolo, J. Appl. Phys. 83 (1998) 2772.
[13] R. Laiho, M. Lakkisto, Philos. Mag. B 48 (1983) 203.
[14] H.P. Christensen, H.P. Jenssen, D.R. Gabbe, M.I.T. Technical Report AD-A162 690, Massachusetts Institute of Technology, Cambridge, MA, 1983.
[15] U. Hommerich, E. Brown, P. Amedzake, S.B. Trivedi, J.M. Zavada, J. Appl. Phys. 100 (2006) 113507.
[16] B. Xu, F. Starecki, D. Paboeuf, P. Camy, J.L. Doualan, Z.P. Cai, A. Braud, R. Moncorge, Ph Goldner, F. Bretenaker, Opt. Express 21 (2013) 5567.
[17] R. Hakim, K. Damak, A. Toncelli, M. Fourati, R. Maalej, J. Lumin. 143 (2013) 233.
[18] J.L. Adam, W.A. Sibley, D.R. Gabbe, J. Lumin. 33 (1985) 391.
[19] H.H. Caspers, H.E. Rast, R.A. Buchanan, J. Chem. Phys. 43 (1965) 43.
[20] A.A. Kaminskii, K. Kurbanov, A.V. Pelevin, Y.A. Polyakova, T.V. Uvarova, Izv. Akad. Nauk. SSSR Neorg. Mater. 24 (1988) 522.
[21] L. Esterowitz, F.J. Bartoli, R.E. Allen, D.E. Wortman, C.A. Morrison, Phys. Rev. B 19 (1979) 6442.
[22] S.R. Bowman, L.B. Shaw, B.J. Feldman, J. Ganem, IEEE J. Quant. Electron. 32 (1996) 646.